Article

Evaluation and Optimization of Interior Circadian Daylighting Performance for the Elderly in Traditional Dwellings: A Case Study in Western Hunan, China

Jixin Liu [ID], Zhe Li, Zuopeng Zhang *, Liang Xie and Jiade Wu

School of Architecture and Art, Central South University, Changsha 410075, China; 221311001@csu.edu.cn (J.L.); lizhe88@csu.edu.cn (Z.L.); liangxie@csu.edu.cn (L.X.); 231301018@csu.edu.cn (J.W.)
* Correspondence: sonzainee@gmail.com; Tel.: +86-186-9227-3326

Abstract: With the implementation of China's rural revitalization strategy, the sustainable preservation of traditional dwellings has become a research priority. Moreover, with the aging population in the countryside increasing, the limited mobility of the elderly may result in them receiving daily corneal illuminance too low for a healthy circadian stimulus. This work aims to explore the relationship between circadian and daylighting design parameters inside traditional dwellings and to develop easy-to-use methods for guiding indoor circadian design in traditional dwellings in western Hunan. Additionally, it seeks to promote the digitalization and informatization of traditional dwellings in western Hunan for preservation purposes, aiming to integrate these efforts with sustainable tourism and community development, which supports the local economy while preserving cultural heritage. The main contributions are as follows: (i) Systematic evaluation of the indoor lighting and circadian status of traditional Miao dwellings in western Hunan. (ii) Simplification and application of the CS and corneal illuminance fitting model for guiding circadian design, especially suitable for indirect indoor circadian aspects of lighting in daylight scenarios. The simplified model provides quick circadian design feedback and promotes healthy circadian concepts. Its accuracy has been verified by fitting it with simulation data from Climate Studio daylighting software. (iii) Exploration of daylighting conditions using simulation software, focusing on ρ' (the area-weighted average of room surface reflectance), ρ (the reflectance of the surface where the first reflection occurs), and the WWR (Window-to-wall ratio) in two different types of traditional dwellings. This also includes defining the dwelling parameter intervals necessary for an appropriate circadian stimulus in traditional Miao dwellings in western Hunan. (iv) The analysis suggests that enhancing ρ' has a greater effect on circadian lighting than WWR, indicating that increasing ρ' should be the preferred method for achieving high-quality and efficient circadian lighting.

Keywords: circadian stimulus (CS); corneal illuminance; elderly; 3D scanning; traditional dwellings; sustainability

1. Introduction

With the advancement of rural revitalization in China, the country has identified 6819 villages of significant conservation value for inclusion in its traditional village registry. Furthermore, around 520,000 structures, including traditional dwellings and temples, have been designated as conservation sites [1]. The digitization and information-based conservation of these traditional dwellings have increasingly attracted academic attention [2,3]. A major ongoing discussion revolves around the effective conservation of these dwellings while maintaining and enhancing their functionality as residences [4]. The challenge is heightened by the traditional dwellings' inability to meet the demands of contemporary living environments, a significant concern given the rural population of about 500 million in China [5]. This fact emphasizes the importance of enhancing indoor comfort in these traditional dwellings.

Globally, the issue of an aging population is escalating, with projections indicating that by 2050, individuals over 65 will constitute 16% of the global population, and those over 80 will see a twofold increase from current figures [6]. In China, this demographic shift is particularly pronounced. From 2010 to 2020, the segments of the population aged 60 and over and 65 and over have risen by 5.44% and 4.63% [7] (Figure 1a), respectively, signaling an intensification of aging issues across all regions [8]. In Xiangxi Tujia and Miao Autonomous Prefecture, the aging crisis is notably acute when compared to global, national, and provincial rates (Figure 1b). Furthermore, the challenge of providing suitable environments for the elderly in China is compounded by the emergence of COVID-19 in 2019, which has turned a spotlight on human health, particularly among the elderly [9,10]. With advancing age, various physiological processes, notably at the circadian level, undergo age-related transformations [11]. This phenomenon has garnered significant research interest, especially regarding the non-visual effects on the elderly population.
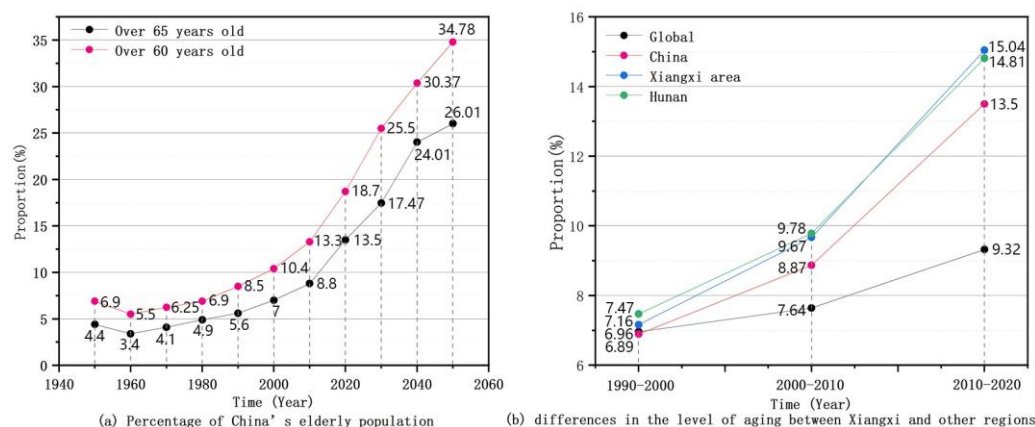

Figure 1. (**a**) Percentage of China's population that is elderly; (**b**) differences in the level of aging between Xiangxi and other regions.

Research on the circadian effects of daylight commenced in 2000. With the discovery of inherent photosensitive retinal ganglion cells (ipRGCs) in the human eye, it became clear that daylight influences not only visual but also non-visual responses. Light entering the retina activates not only the visual photo transducer cells of the optic rod and cone cells but also the ipRGCs. These cells convert non-visual light signals into biological signals, which are then transmitted via the suprachiasmatic nucleus (SCN) to the pineal gland [12]. This gland is crucial for melatonin production and circadian regulation [13]. The melatonin-mediated mechanism serves as a foundational aspect in studies exploring circadian responses to daylight [14]. Medical research indicates that higher illumination levels more effectively inhibit melatonin production, thus influencing the circadian stimulus [15]. However, the non-visual response to daylight is not solely dependent on light intensity. Factors such as time of day [16] and daylight duration [17,18] also play significant roles. The human biological clock averages a daily cycle of 24.2 h [19]. This cycle is synchronized with the astronomical 24-h cycle through the early morning peak of the circadian resetting period [18]. This synchronization is essential for optimal physiological and biological functioning.

Elderly individuals, a distinct social demographic, experience reduced exposure to blue light due to lens yellowing, making them more reliant on daylight compared to other groups [20]. Changes in contemporary lifestyles often result in the elderly spending upwards of 80% of their time indoors, a factor attributed to declining physical functions. This indoor predominance leads to inadequate circadian stimulation, potentially causing various health issues such as sleep disorders [21,22], diabetes [23], Alzheimer's disease [24], seasonal affective disorder (SAD), and even cancer [25]. Adequate lighting plays a crucial role in regulating their biological clocks by modulating melatonin secretion and ameliorating conditions such as sleep disturbances, anxiety, and depression [26]. Moreover,

daylight therapy, an affordable and safe non-pharmacological approach, presents a promising option for augmenting or replacing dementia treatments [27]. Research indicates that daylight significantly influences mood [28], circadian regulation [16], pupillary reflexes [29], alertness [30], and overall health [31–33] in the elderly. Consequently, ordinary visual daylight metrics are insufficient to meet the requirements; indoor daylighting design for this group should account not only for visual needs but also for their non-visual and health-related requirements.

Recent advancements in the study of non-visual effects of indoor daylight environments have led to the development of models quantifying daylight's impact on the circadian stimulus. *The Circadian Stimulus* (CS) model [34] by Rea et al. and *the Equivalent Melanopic Lux* (EML) model [35] are predominant in this field, finding extensive application in medical and optical research. This paper utilizes the CS model to quantify the circadian stimulus [36], defining CS value as the percentage reduction in melatonin production [37]. Research involving Alzheimer's disease patients and the elderly indicates that daylight interventions with a minimum early-day CS value of 0.3 effectively enhance the circadian stimulus and sleep quality [38]. Research by Dai et al. suggests that the daily daylight exposure currently received by individuals may be insufficient. Even with the high circadian stimulus of the CIE D65 spectra, a minimum of 180 lx corneal illuminance [39] is required. Achieving such illuminance levels is feasible near windows but poses challenges in rooms farther from windows [40].

Research indicates that multiple factors influence the circadian stimulus in indoor daylight environments. These factors include WWR [41], interior reflectance ratio [42], shading, and viewing angle [43,44]. Studies by Cai et al. [42] and Yao et al. [45] have demonstrated that when considering only internally reflected daylight, wall reflectance significantly impacts corneal illuminance. Additionally, high corneal illuminance from direct indoor daylight often results in uncomfortable glare [14]. Therefore, focusing on enhancing the indirect component of corneal illuminance emerges as a promising strategy in design.

While most studies on circadian stimuli have concentrated on urban buildings, traditional dwellings, particularly in areas with unique climates, lifestyles, and dwellings materials, necessitate specialized and practical evaluation methods. These methods should assess the circadian levels and propose improvements, offering prompt design feedback for diverse settings. This research focuses on the conservation and modernization of traditional Miao dwellings in the Xiangxi Tujia and Miao Autonomous Prefecture, China. It involves evaluating and analyzing the indoor daylight environment for the elderly, specifically in terms of circadian aspects. This evaluation serves as a guide for circadian-centric design and seeks to discover effective strategies for enhancing indoor circadian conditions in the traditional dwellings of western Xiangxi. On a sustainable level, maximize the use of natural light to reduce energy consumption and promote environmental health.

1. Digital models of traditional dwellings in western Hunan were created using 3D laser scanning and drone tilt photography. Subsequently, a lighting simulation model was constructed in Rhino 7.0. The simulation results from Climate Studio were then cross-verified with actual field-measured illuminance data, affirming the reliability of Climate Studio's simulations.
2. Daylighting simulations, incorporating both dynamic and static approaches, were executed to evaluate the CS levels in the interiors of two distinct dwelling types (L-type and I-type) common among the Miao ethnic group in western Hunan.
3. Simplified the fitting model of CS with WWR and reflectance, and verified its accuracy.
4. The study conducted a statistical analysis and quantitative simulation of the WWR and reflectance of interior materials used in traditional Miao dwellings located in western Hunan. The aim was to establish the necessary dwellings parameter ranges for an appropriate circadian stimulus.

2. Research Object

This study is focused on the traditional villages of the Miao ethnic group, which have meticulously preserved their traditional architectural designs and cultural heritage. Among the five designated batches of "Chinese traditional villages", Xiangxi Tujia and Miao Autonomous Prefecture boast an impressive total of 172 traditional villages. Currently, research concerning the traditional dwellings in Xiangxi has primarily centered around their spatial morphology and the indoor humid and hot environments. However, there has been a notable lack of research regarding the daylight environment. Field surveys have revealed that the majority of traditional dwellings in the region suffer from inadequate indoor lighting conditions, necessitating suitable renovations. In this study, Zhushan Village in Fenghuang County is selected as a representative Miao traditional village research object (Figure 2). This village typifies the living environment of the Miao people in western Hunan, offering insight into their current circumstances due to its remote location, well-preserved landscape, and the predominant occupancy of elderly residents.
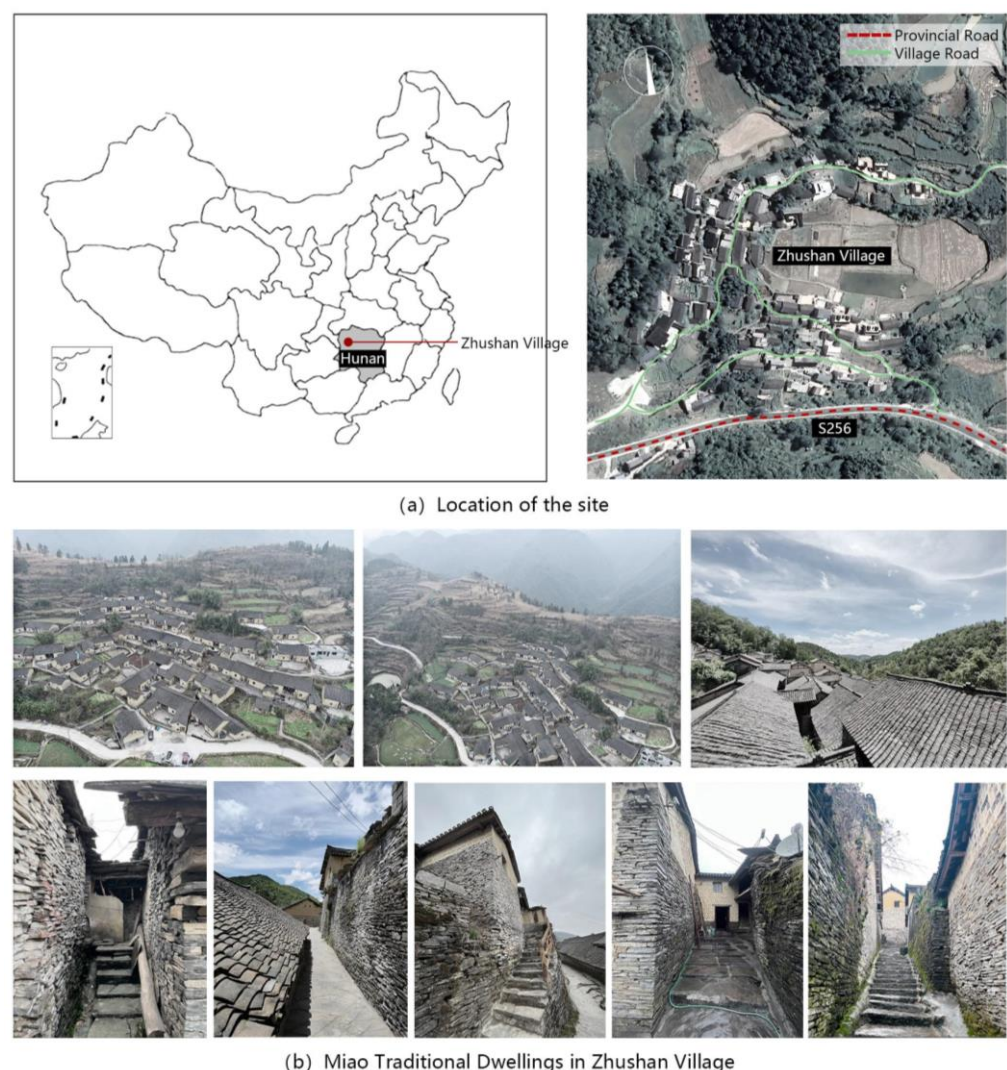

(a) Location of the site

(b) Miao Traditional Dwellings in Zhushan Village

Figure 2. (**a**) Location of the site; (**b**) Miao Traditional Dwellings in Zhushan Village.

This paper examines traditional Miao dwellings, focusing on L-type and I-type structures where the hall dwellings is central, surrounded by other spaces such as bedrooms, fireplace, storage, toilet, and kitchen. These components are crucial for the Miao's living arrangement, resembling a "swallowing mouth" layout. This study primarily investigates the indoor daylight environment of these dwellings to propose daylight-

ing optimization strategies. By analyzing the indoor activity patterns of Hmong elders (Figure 3), who primarily use the living room, fire pit, and bedroom, the research aims to enhance their limited exposure to daylight, improving their health and physiological circadian. The methodology includes a thorough analysis followed by simulations and evaluations of the daylighting enhancements. The objective is to lay groundwork for further research and, through collaboration with local authorities, implement these daylighting solutions effectively.
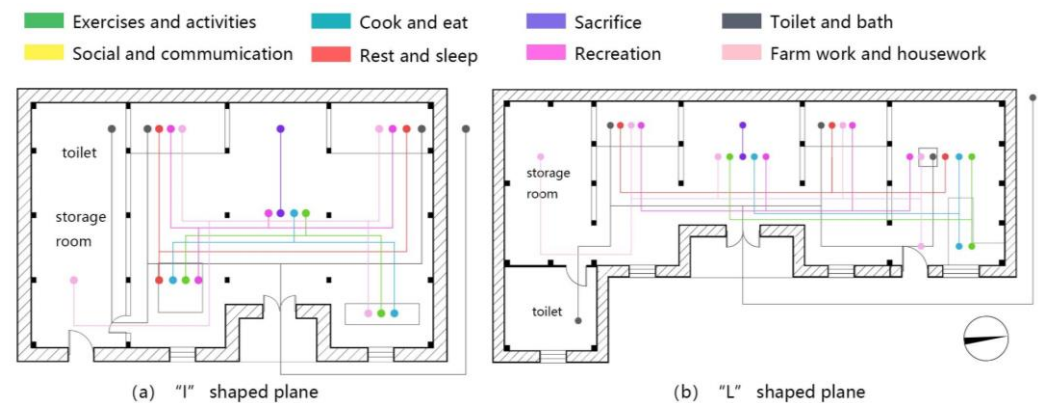

Figure 3. Daily activities of the elderly: (**a**) "I"-shaped plan; (**b**) "L"-shaped plan.

3. Research Methods

3.1. Survey

Unstructured interviews and illumination assessments were carried out in Zhushan Village over a two-week period in the peak of summer 2023, specifically from 20 June to 4 July. These interviews uncovered that the village predominantly dwellings residents aged 60 and above. In the study, 49 households were involved, housing 82 permanent residents, out of which 76 (representing 92%) were elderly. This demographic profile is representative of most Hmong villages. While the focus of this study is on the indoor daylight conditions of traditional Hmong dwellings, it also intricately examines the living conditions of these elderly residents who reside there throughout the year.

3.2. Model Establishment and Validation

3.2.1. Modeling Process

Given the abundance of traditional dwellings in Zhushan Village, conducting exhaustive ground mapping, detailed modeling, and comprehensive quantitative analysis on each dwelling presents significant challenges. Therefore, the study's focus was refined to include only a selection of the most representative dwellings. This decision was further influenced by the limited availability of well-maintained homes and the small number of villagers amenable to participating in field surveys. Consequently, the research narrowed its scope, concentrating on a subset of traditional Hmong dwellings that met specific criteria suitable for in-depth quantitative analysis.

(1) There are long-term residents in the residence, and we can understand their visual task needs.

(2) The dwellings have not been seriously damaged or constructed, and their basic appearance has been maintained.

(3) The daylighting system of the residence is representative and can reflect and represent the daylighting situation of other residences in the village.

For the quantitative simulation, two geometric models were chosen reflecting the architectural styles of the Miao people's traditional dwellings in western Hunan. The L-type dwelling selected for quantitative analysis is Wu Jianlong's self-constructed residence, situated in the southern area of Zhushan Village, with its 'swallowing mouth' oriented eastward. Similarly, for the I-type dwelling, the chosen model is the self-constructed

residence of Long Qubing, located in the village's western part, also featuring an east-facing swallowing mouth (Figure 4).
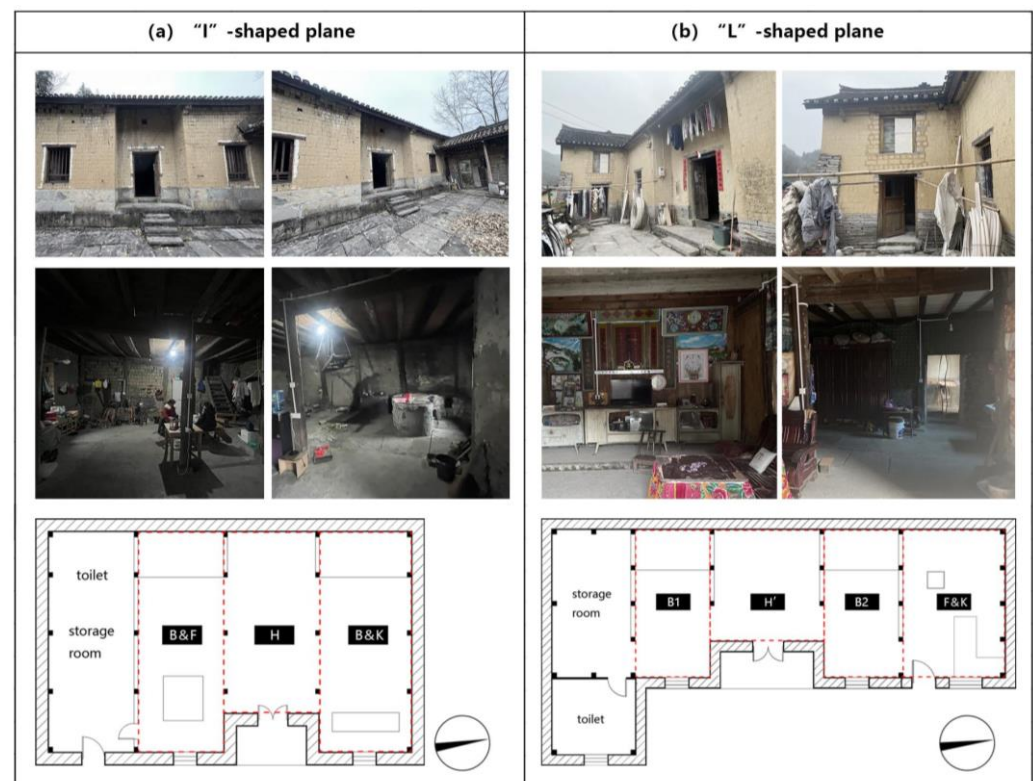

Figure 4. Typical traditional dwelling plan types of the Miao nationality in Zhushan Village; each plan shows a labeled overhead view (H = hall, B = bedroom, F = fire pit, K = kitchenette); (**a**) "I"-shaped plan (**b**) "L"-shaped plan.

While traditional manual mapping remains a renowned architectural graphic method in Chinese architecture, it has limitations such as inefficiency, a monotonous mode of expression, restricted capabilities in 3D transformation, and variable accuracy. The advancement of architectural heritage into the digital and information age has witnessed the advent of novel mapping technologies, including 3D laser scanning and drone-based oblique photography, which are progressively enhancing the mapping system.

This research delineated the creation of a 3D model into four distinct phases (Figure 5). Initially, comprehensive tilt photography of Zhushan Village was executed, and the Context Capture 2023 was utilized to transform POS data and imagery into a 3D representation encompassing dwellings, terrain, roads, and vegetation. Subsequently, the Trimble X7 3D laser scanner was employed to acquire point cloud data from multiple locations within traditional housing units, and Trimble Real works 12.0 was used to merge this data, producing 3D point cloud models [46]. Due to the dense arrangement and extensive roof areas of traditional dwellings in Zhushan Village, roof scanning posed challenges. To address this, the 3D laser scanner captured point cloud data for the structures beneath the roofs, and UAV tilt photography-derived models supplemented the roof data. The third phase involved reverse modeling in Rhino 7.0, integrating both the tilt photography and point cloud models (Figure 5(3)). The final phase entailed manual correction of any prominent errors.
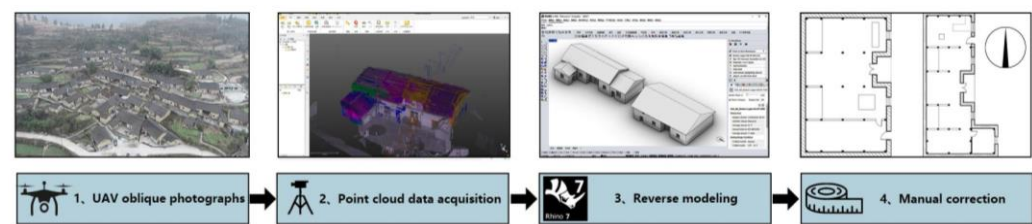
Figure 5. Steps of modeling.

3.2.2. Validation

The primary method for verifying and enhancing the reliability of the numerical model involves model validation [47]. The 3D model generated for this study incorporated the optical properties of materials from EnergyPlus [48] and the ClimateStudio material library and climate data from the CSWD in Xiangxi Tujia and Miao Autonomous Prefecture, Hunan, China, inputted into Climate Studio [49]. Reflectance data for each material were also included (Table 1).

Table 1. Measured material properties.

Material	Position	Reflectance	Material	Position	Reflectance
Rammed earth	Upper end of exterior wall	21.7%	China Fir	Structure	21.1%
Stone	Lower end of exterior wall	25.3%	Yellow paint wood	Ceiling	29.6%
Red paint wood	Column, Interior wall	19.6%	Cement	Interior flooring	18.1%
Grey Tile	Roof	7.3%	Brown paint wood	Door	18.3%

In the field of illuminance measurement, the methods delineated in the Chinese standard GB/T 5699-2017 (Method of Daylighting Measurements) [50] were employed. The chosen instrument for this task was the JTG01 illuminance meter, which boasts a measurement range of 0.1–100,000 lx and a measurement accuracy surpassing ±4%. In adherence to the guidelines of GB/T5699-2017, it is recommended for researchers to don dark attire during the measurement process. This practice minimizes the impact of clothing reflections on the measurement outcomes. The protocol also advises conducting the illuminance measurement at a time of day when the illuminance levels are notably stable, specifically between the hours of 10:00 a.m. and 2:00 p.m. In Bamboo Hill Village, the sun's altitude angle is considerably high during this interval, thereby ensuring that the illuminance within a room remains relatively consistent over a short time span. This consistency is beneficial for researchers aiming to conduct illuminance measurements at various indoor locations simultaneously at a specific point in time. Consequently, the illuminance measurements were scheduled for 24 June 2023, at 1:00 p.m. For the selection of measurement points within the dwellings, 40 intersections of the column network, each at a height of 750 mm (Figure 6), were identified in accordance with GB/T 10000-1988 (Human Dimensions of Chinese Adults) [51] and GB/T 5699-2017 (Method of Daylighting Measurements) [50]. This selection criteria facilitated the clear identification of these points on the model. Areas such as toilets and storage rooms were exempted from setting measurement points due to the low illuminance levels in these spaces, which were deemed insufficiently contributive for validation purposes.
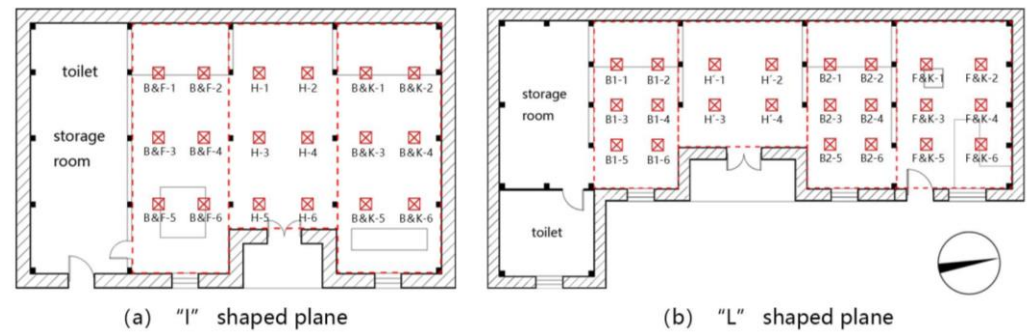
Figure 6. The distribution of measuring points.

In our analysis to discern the discrepancies between simulated and measured values, we utilized two error analysis metrics, specifically relative mean bias error (*MBErel*) and relative root mean squared error (*RMSErel*). These metrics are prevalently applied in the study of lighting environments. We consider calculated values within a 20% margin to be credible [52,53]. (Figure 7) presents the scatter plots comparing E (simulation) with E (measurement) for two typical dwellings. In this context, E (simulation) represents the simulated illuminance values, and E (measurement) corresponds to the actual measured illuminance values. Across both data sets, E (simulation) and E (measurement) are aligned along the y = x reference line, demonstrating *MBErel* values of −3.7% and −3.1% and *RMSErel* values of 12.3% and 18.2%, respectively. All these values fall under the 20% error threshold. Consequently, the simulated values obtained via Climate Studio exhibit a commendable consistency with the measured values, thereby reinforcing their accuracy and reliability in the context of this study.
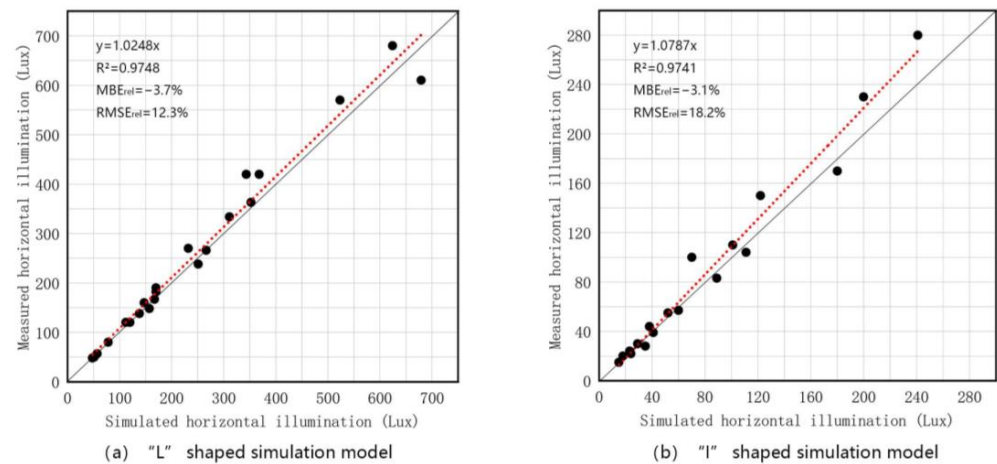

Figure 7. Scatter plots of E (simulation) and E (measure).

3.3. Circadian Evaluation System

In the spectral sensitivity model for human circadian, the measurement unit for circadian light (CL_A) [37], as proposed by Rea et al., represents the spectrally weighted flux per unit area from all photosensitizing pigments known to contribute to circadian spectral sensitivity. The formula for calculating circadian light (CL_A) is outlined as follows:

$$CL_A = \begin{cases} 1548\left[\int Mc_\lambda E_\lambda d\lambda + \left(a_{b-y}\left(\int \frac{S_\lambda}{mp_\lambda}E_\lambda \mathrm{d}\lambda - k \int \frac{V_\lambda}{mp_\lambda}E_\lambda \mathrm{d}\lambda\right) - a_{\mathrm{rod}}\left(1 - e^{\frac{-\int V'_\lambda E_\lambda \mathrm{d}\lambda}{\mathrm{RodSat}}}\right)\right)\right], \\ \qquad \text{if } \int \frac{S_\lambda}{mp_\lambda}E_\lambda \mathrm{d}\lambda - k \int \frac{V_\lambda}{mp_\lambda}E_\lambda \mathrm{d}\lambda > 0 \\ 1548\int Mc_\lambda E_\lambda \mathrm{d}\lambda, \text{if } \int \frac{S_\lambda}{mp_\lambda}E_\lambda \mathrm{d}\lambda - k \int \frac{V_\lambda}{mp_\lambda}E_\lambda \mathrm{d}\lambda \leq 0 \end{cases} \qquad (1)$$

CL_A: *circadian light*
E_λ: *light source spectral irradiance distribution*
Mc_λ: *melanopsin (corrected for crystalline lens transmittance)*
S_λ: *S-cone fundamental*
mp_λ: *macular pigment transmittance*
V_λ: *photopic luminous efficiency function*
V'_λ: *scotopic luminous efficiency function*
$RodSat$: *half-saturation constant for bleaching rods* = 6.5 W/m^2
k = 0.2616
a_{b-y} = 0.7000
$a_{\rm rod}$ = 3.3000

Bellia et al. further refined this process by introducing a linear model correlating CL_A with E_{cor} [54]. This model simplifies the calculation of CL_A, making it applicable to a broad range of light sources, including daylight in the D65 spectrum, and is expressed as follows:

$$CL_A = \begin{cases} \left(\dfrac{1622 \int C(\lambda)E(\lambda)\mathrm{d}\lambda}{683 \int V(\lambda)E(\lambda)\mathrm{d}\lambda} - 0.67 \right) E_{cor} \\ \text{If } opp = \int S(\lambda)E(\lambda)\mathrm{d}\lambda - 0.33 \int V(\lambda)E(\lambda)\mathrm{d}\lambda \geq 0 \\ \left(\dfrac{1622 \int C(\lambda)E(\lambda)d\lambda}{683 \int V(\lambda)E(\lambda)d\lambda} + 0.11 \right) E_{cor} \\ \text{If } opp = \int S(\lambda)E(\lambda)\mathrm{d}\lambda - 0.33 \int V(\lambda)E(\lambda)\mathrm{d}\lambda < 0 \end{cases} \tag{2}$$

CL_A: *circadian light*
E_{cor}: *corneal illuminance value*
$C(\lambda)$: *circadian spectral sensitivity function*
$E(\lambda)$: *spectral irradiance distribution*
$\mathrm{d}\lambda$: *Spectral distance between two wavelengths*
$V(\lambda)$: *photopic visual sensitivity*
$S(\lambda)$: *sensitivity function of the short-wavelength cone*
opp: *represents the blue-yellow channel response (positive for the 'blue' response and negative for the 'yellow' response)*

Advancements in this field led Rea et al. to further distill the relationship between the Circadian Stimulus (CS) and CL_A [34], particularly during the early part of the day, termed the "peak of the circadian resetting period" (8:00–10:00 a.m.). The revised equation for converting CS to CL_A during this timeframe is as follows:

$$CS = 0.7 - \frac{0.7}{1 + \left(\frac{CL_A}{355.7} \right)^{1.1026}} \tag{3}$$

3.3.1. Corneal Illuminance Simulation

The simulation process for corneal illuminance encompassed two approaches: a dynamic simulation over the entire year and a static simulation at a specific moment, aiming to gather a more exhaustive spatial data set.

In the dynamic daylight simulation, the CS is categorized into four ranges: 0–0.14 (indicating no wakefulness), 0.14–0.3 (insufficient wakefulness), 0.3–0.5 (adequate wakefulness), and 0.5–0.7 (wake saturation) [55]. To facilitate an intuitive analysis of CS variations throughout the year, this study segments the simulation timeline based on the vernal equinox, summer solstice, autumnal equinox, and winter solstice, computing the duration percentages for each CS range during the different seasons. Furthermore, considering the variability between areas near and far from the window, the space is bifurcated into two zones for analysis. The CS in each zone is then assessed to gauge the impact of seasonal shifts on wakefulness levels. Additionally, the coefficient of variation (Cv) for each CS range in distinct seasons is calculated to understand the seasonal fluctuation of CS.

In the static daylight simulation, the period exhibiting the lowest CS was identified from the dynamic simulation results. The chosen weather condition for this phase was the standard CIE overcast day, representing the most challenging daylight scenario within the space over a year. The simulation time was strategically set during the peak of the circadian resetting period (8:00–10:00 a.m.) [40]. During this interval, the Avg E_{cor} and CS for each area were calculated. A situation where the daylight (D65 spectrum) ensured an E_{cor} of at least 180 lx, equating to a CS of 0.3 or higher for a minimum of one hour, was considered to fulfill the requirements for an adequate circadian stimulus [39].

E_{cor} serves as the foundational data for subsequent analysis. Considering that elderly individuals spend extended periods sitting indoors, the simulation plane's height was set at 750 mm above the ground, aligning with the average eye height of seated Chinese adult men and women as specified in GB/T 10000-1988 (Human dimensions of Chinese adults) [51]. In these simulation planes, sensors were arranged following a 200 mm $\times$ 200 mm grid matrix (Figure 8a,b). The data collected from these sensors were then processed and analyzed using Climate Studio.
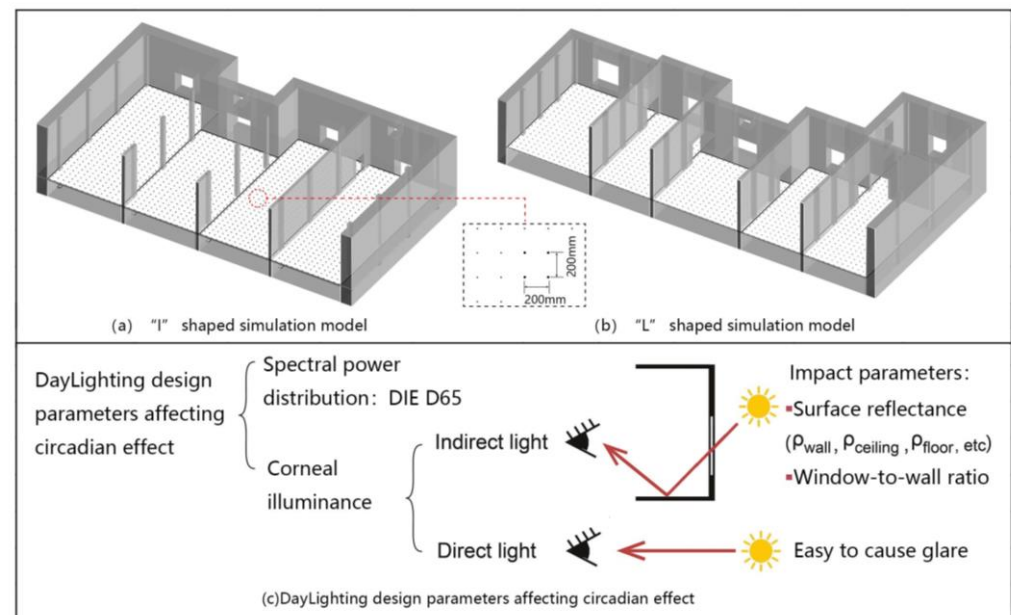

Figure 8. (**a**) "I"-shaped simulation model (**b**) "L"-shaped simulation model. (**c**) Day Lighting design parameters affecting circadian effect.

3.3.2. Circadian-Stimulus-Based WWR and Reflectance Design

Enhancing CS can be achieved by increasing the Ecor, which consists of two components. $E_{cor\,(i)}$ represents the light reflected at least once in the space before reaching the eye, while $E_{cor\,(d)}$ is the light directly incident on the eye. It is important to note that increasing $E_{cor\,(d)}$ significantly might result in a high amount of direct light entering the eye, potentially causing glare. On the other hand, augmenting $E_{cor\,(i)}$ can mitigate such risks [14].

To investigate the impact of various parameters in a space on $E_{cor\,(d)}$ and $E_{cor\,(i)}$, Yao and colleagues developed a model based on factors such as k, WWR, ρ, and ρ' [42,45]. The findings from Yao et al.'s model indicate that $E_{cor\,(i)}$ relationship with ρ' is super-linear and sub-linear with WWR, highlighting the predominant influence of ρ' in enhancing $E_{cor\,(i)}$, E_{cor}, CL_A, and CS (Figure 8c). The formula for this model is as follows:

$$E_{cor} = E_{cor(d)} + E_{cor(i)} = E_{cor(d)} + k \cdot WWR \cdot \frac{\rho}{1 - \rho'} \tag{4}$$

E_{cor}: *corneal illuminance value*
$E_{cor(d)}$: *The direct portion of* E_{cor}
$E_{cor(i)}$: *The indirect portion of* E_{cor}
k: *A constant determined by factors such as sky condition, window direction, and total room surface area*
WWR: *Window-to-wall ratio*
ρ: *The reflectance of the surface where the first reflection occurs*
ρ': *The area-weighted average of room surface reflectance*

To achieve the target CS value of 0.3 or higher in indoor spaces and minimize glare from elevated $E_{cor\,(d)}$, enhancing $E_{cor\,(i)}$ can be effective. This enhancement involves increasing both the ρ' and the Window to Wall Ratio (*WWR*). Given the super linear correlation between $E_{cor\,(i)}$ and ρ' (Equation (4)), the latter is more influential in determining the optimal mix of ρ' and *WWR* for subsequent simulations. These simulations, conducted in Climate Studio, were based on static, overcast conditions to ascertain the necessary parameters for meeting the basic CS under the most challenging weather scenarios. (Figure 8a,b) illustrates the simulation plane where various parameter combinations were tested and evaluated to identify those meeting the CS threshold of 0.3 or more.

3.3.3. Simplified Fitting Models

To delineate the impact of individual parameters in a space on CS, this study has refined the mathematical models proposed by Yao, Rea, and Bellia. This refinement led to a streamlined model of CS that incorporates variables such as k', WWR, ρ, and ρ'. The model is represented by the following formulae:

$$CS = CS_{(d)} + CS_{(i)} = CS_{(d)} + k' \cdot WWR \cdot \frac{\rho}{1 - \rho'} \tag{5}$$

CS: *Circadian stimulus*
$CS_{(d)}$: *The direct portion of CS*
$CS_{(i)}$: *The indirect portion of CS*
k': *A constant determined by factors such as sky condition, window direction, and total room surface area*
WWR: *Window-to-wall ratio*
ρ: *The reflectance of the surface where the first reflection occurs*
ρ': *The area-weighted average of room surface reflectance.*

4. Results and Discussion
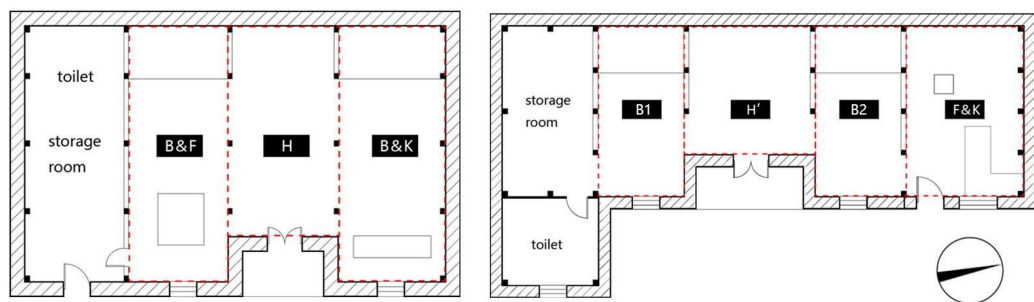
4.1. Corneal Illuminance Simulation

4.1.1. Annual Corneal Illuminance Simulation

Table 2 presents the annual daylight simulation and statistical outcomes for key areas within a standard Zhushan village residential dwellings (L & I type). The table employs varied saturation levels of a consistent color scheme to denote the relative scale of values within identical categories. For seasonal variations in CS intervals, the table calculates and displays average figures for each area collectively.

Analysis of (Table 2) reveals that seasonal changes impact CS intervals differently. The Cv data shows Cv Avg $CS_{0.5-0.7}$ as the highest, followed by Cv Avg $CS_{<0.14}$, Cv Avg $CS_{0.14-0.3}$, and Cv Avg $CS_{0.3-0.5}$. This pattern suggests a minimal influence of seasonal shifts on the duration of optimal CS intervals. Notably, Avg $CS_{0.5-0.7}$ experiences the most significant seasonal fluctuation, rarely exceeding 10%time coverage in most spaces, except during spring and summer. This implies a marginal effect of seasons on room saturation levels of CS. Furthermore, the noticeable winter increase in Cv Avg $CS_{<0.14}$ across all units indicates that older adults indoors may struggle to receive a sufficient circadian stimulus.

Table 2. Summary of the percentage value of each CS interval in each season for each functional area.

Zone	Season	Avg. $CS_{<0.14}$	Avg. $CS_{0.14-0.3}$	Avg. $CS_{0.3-0.5}$	Avg. $CS_{0.5-0.7}$
B&F	Spring	58.15%	27.63%	11.38%	2.84%
	Summer	49.96%	32.08%	13.25%	4.71%
	Autumn	68.46%	21.56%	8.72%	1.26%
	Winter	73.74%	19.16%	6.24%	0.86%
	Cv	16.96%	23.33%	30.97%	72.43%
H	Spring	31.36%	40.49%	20.85%	7.30%
	Summer	20.71%	46.85%	22.52%	9.92%
	Autumn	43.97%	35.76%	14.06%	6.21%
	Winter	56.55%	27.70%	13.15%	2.60%
	Cv	40.68%	21.40%	26.80%	46.63%
B&K	Spring	55.75%	32.83%	9.26%	2.16%
	Summer	48.05%	35.42%	12.45%	4.08%
	Autumn	63.46%	24.58%	10.04%	1.92%
	Winter	75.72%	14.49%	9.20%	0.59%
	Cv	19.42%	35.17%	14.88%	65.75%
B-1	Spring	39.48%	40.24%	15.80%	4.48%
	Summer	26.15%	44.34%	22.60%	6.91%
	Autumn	49.45%	32.97%	13.57%	4.01%
	Winter	69.29%	19.56%	8.73%	2.42%
	Cv	39.42%	31.74%	37.97%	41.72%
H′	Spring	23.66%	28.45%	33.46%	14.43%
	Summer	16.29%	25.36%	40.83%	17.52%
	Autumn	27.55%	35.82%	27.02%	9.61%
	Winter	29.21%	40.73%	26.27%	3.79%
	Cv	23.78%	21.41%	21.24%	52.85%
B-2	Spring	31.47%	39.02%	23.70%	5.81%
	Summer	25.74%	38.60%	26.23%	9.43%
	Autumn	41.52%	30.19%	23.04%	5.25%
	Winter	60.47%	19.04%	17.72%	2.77%
	Cv	38.30%	29.56%	15.77%	47.26%
F&K	Spring	21.65%	40.80%	31.03%	6.52%
	Summer	17.34%	48.29%	24.71%	9.66%
	Autumn	19.32%	39.03%	32.92%	8.73%
	Winter	34.45%	36.21%	26.18%	3.16%
	Cv	33.25%	12.56%	13.56%	41.17%
Schematic plan					

Significant shifts in the four CS intervals primarily occur between the seasons of summer to fall and winter to spring. Consequently, these CS variations correlate strongly with the solar position relative to the equator. As the direct sunlight position shifts, the peak solar elevation angle at midday in Zhushan Village adjusts accordingly, impacting the CS experienced by residents. Located in the northern hemisphere, specifically in Fenghuang County's Zhushan Village, Xiangxi, this pattern indicates that the circadian stimulus (CS) is most lacking around the winter solstice, particularly in the period surrounding December 22nd.

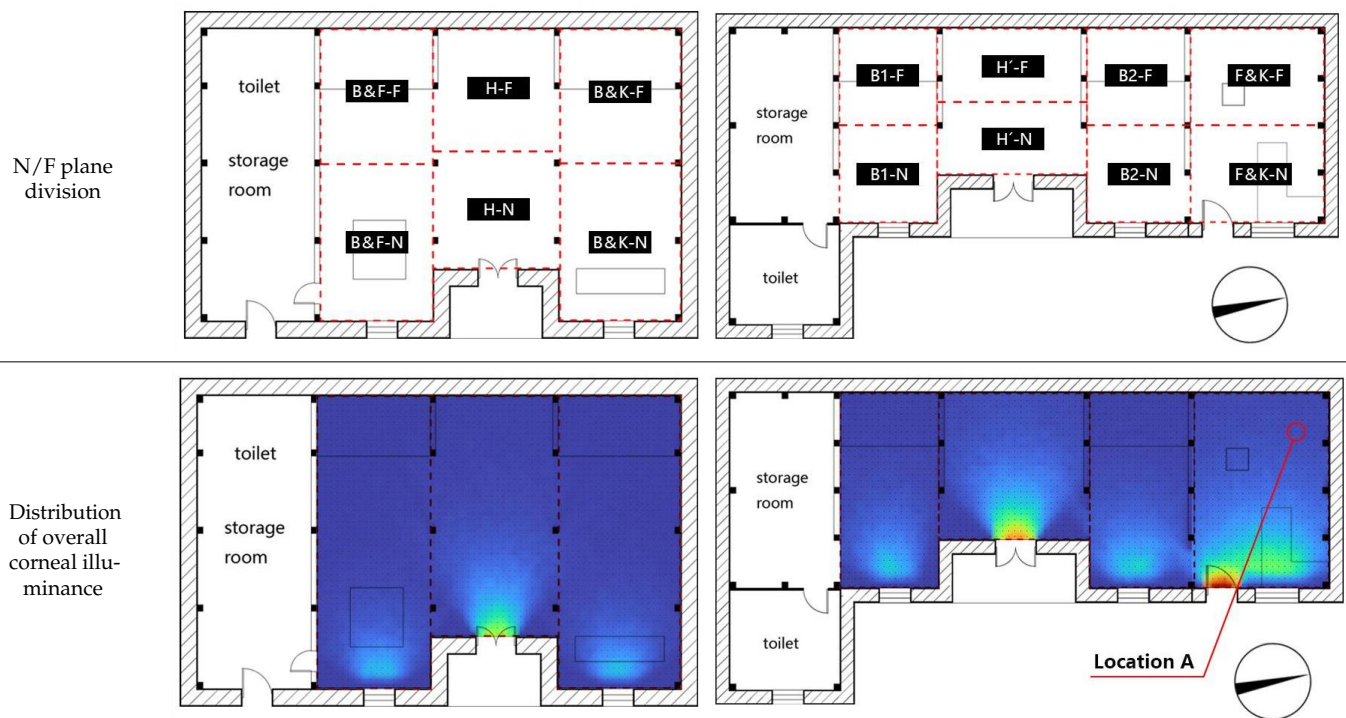4.1.2. Point-in-Time Corneal Illuminance Simulation

To accurately assess the discrepancy between actual and ideal CS values during the least favorable circadian stimulus period, a daylight simulation under CIE standard overcast conditions was performed, a prevalent method in this field [56]. This simulation specifically used 9:00 a.m. on 22 December 2023 as the reference time, notable for both its minimal natural illumination and as a critical point in the circadian resetting cycle [40]. Future redesign efforts will build upon these simulation conditions. For enhanced granularity in data, spaces were bifurcated into two zones, 'near window' and far window, based on a central line running the depth of each area. These zones are designated as N for near window and F for far window (Table 3).

Table 3 illustrates the parameter settings for each area and the distribution of Avg E_{cor} in primary activity zones. In the vicinity of windows, Avg E_{cor} ranges from 29 to 158 lux, correlating to CS values between 0.06 and 0.27. Conversely, areas distant from windows show Avg E_{cor} values from 5 to 28 lux, with CS values ranging from 0.01 to 0.06. Daylight exposure, specifically D65 spectrum, achieving an average E_{cor} of at least 180 lux (CS $\geq$ 0.3) for a minimum of one hour, is deemed sufficient for circadian stimulation [39]. The analysis indicates that, despite the substandard indices in both near and far window regions, Avg E_{cor} tends to increase with the enhancement of WWR and ρ'.

All indicators in the near window region are generally larger than those in the far window region. The substantial difference between these regions, particularly in terms of daylight data, can be mainly attributed to the direct light influencing the E_{cor} in the near window region under identical sky and spatial model parameters. This situation ensures that a sufficient circadian stimulus is achieved even when both ρ and $\rho^{\hat{}}$ are at lower levels. This phenomenon indicates that the Window to Wall Ratio (WWR) has a certain influence on the circadian stimulus. As the spatial depth increases, the role of indirect light in the space becomes less dominant due to the limitations set by the model parameters. This leads to a lower circadian stimulus in the far window region. To elaborate, in the case of 'location A', as indicated in (Table 3), the corneal illuminance primarily comes from indirect light, which has undergone at least one reflection within the room. Specifically, in this scenario, the E_{cor} at location A registers at 18 lux, markedly lower than the optimal level of 180 lux, thereby failing to provide an adequate circadian stimulus. However, it is noteworthy that these areas lacking a circadian stimulus are the primary activity zones for the Miao elderly in western Hunan. Therefore, to meet the basic circadian needs of the elderly during daytime, these areas might require the addition of RGBW LED artificial light sources capable of simulating natural daylight [57,58]. A properly managed circadian daylighting system should ensure adequate coverage across most of the activity areas. For rooms with deeper spaces, increasing the material surface reflectance and enhancing the WWR could be potential strategies to improve the corneal illuminance.

Table 3. Simulation and statistical results for point-in-time illuminance quantity in each functional area; N/F plane division, Distribution of overall corneal illuminance.

Zone Number	Window Area [m²]	Wall Area [m²]	Window-to-Wall Ratio	Daylighting Mode	ρ	ρ′	Geometry Center-to-Window Distance [m]	Avg. *Evor* [lux]	Avg. CS
B&F-N	1.1	16.8	0.07	Direct	18.10%	21.87%	2.80	30	0.06
B&F-S				Indirect			7.55	6	0.01
H-N	3.6	19.5	0.18	Direct	18.10%	21.88%	2.10	61	0.12
H-S				Indirect			6.20	9	0.02
B&K-N	1.1	16.8	0.07	Direct	18.10%	21.86%	2.80	29	0.06
B&K-S				Indirect			7.55	5	0.01
B1-N	1.2	14.0	0.09	Direct	18.10%	21.89%	2.10	50	0.10
B1-S				Indirect			5.20	11	0.02
H´-N	3.6	22.0	0.16	Direct	18.10%	22.12%	1.25	96	0.18
H´-S				Indirect			3.80	28	0.06
B2-N	1.2	13.6	0.09	Direct	18.10%	21.89%	2.10	64	0.13
B2-S				Indirect			5.20	12	0.03
F&K-N	4.2	20.1	0.21	Direct	18.10%	22.57%	2.10	158	0.27
F&K-S				Indirect			5.20	28	0.06

N/F plane division	
Distribution of overall corneal illuminance	

4.2. Circadian-Stimulus-Based WWR and Reflectance Design, Validation of Simplified Fitting Models

4.2.1. Circadian-Stimulus-Based WWR and Reflectance Design

This study adheres to the indoor surface reflectance range as recommended by EN 12464-1-2011 (Lighting of Work Places) [59] and adopts the Window to Wall Ratio (WWR) as per the guidelines of GB 50189-2005 (Design Standard for Energy Efficiency of Public Buildings) [60]. These standards were utilized to select a reasonable range for both indoor reflectance and WWR (Table 4). In the original model parameters, Table 5 illustrates the area of each surface.

Table 4. Recommended values of room surface reflectance from EN12464-1 2011; Recommended values of window-to-wall ratio from GB50189-2005.

Room Surface Reflectance	
Item	**Range**
Ceiling	0.7 to 0.9
Walls	0.5 to 0.8
Floor	0.2 to 0.4
Window-to-Wall Ratio	
Item	**Range**
Window-to-wall ratio	0 to 0.7

Table 5. Area of each surface under three window-to-wall ratios.

Parameters	WWR	S_{Walls}	S_{Window}	$S_{T-Walls}$	S_{Floor}	$S_{Ceiling}$	S_{Total}
I: current value	11%	53.1	5.8	178.6	112.8	112.8	404.2
	30%	53.1	15.9	168.5	112.8	112.8	394.1
Preset of type I	50%	53.1	26.6	157.8	112.8	112.8	383.4
	70%	53.1	37.2	147.2	112.8	112.8	372.8
L: current value	15%	69.7	10.2	193.2	93.6	93.6	380.4
	30%	69.7	20.9	182.5	93.6	93.6	369.7
Preset of type L	50%	69.7	34.9	168.5	93.6	93.6	355.7
	70%	69.7	48.8	154.6	93.6	93.6	341.8

(Table 3) reveals that as space depth increases, areas near far windows receive little direct sunlight. Consequently, the significance of indoor surface reflectance escalates for adequate circadian stimulation. Corresponding to the ranges suggested in (Table 4), additional tiers in indoor reflectance are established. Specifically, we selected three WWR tiers (0.3, 0.5, and 0.7); three wall reflectance tiers (0.4, 0.6, and 0.8); three ceiling reflectance tiers (0.4, 0.6, and 0.8); and two floor reflectance tiers (0.2 and 0.4). This results in 54 possible combinations ($3 \times 3 \times 3 \times 2$) of reflectance and WWR, detailed as follows (Table 6).

The simulation, set at 9:00 a.m. on December 22 under CIE standard cloudy conditions, concentrated on the seven principal activity spaces. (Figure 9) depicts the distribution of overall CS within these main activity areas in two typical dwellings, influenced by varying combinations of WWR and ρ. The findings are as follows: (1) There is a discernible decreasing trend in CS, moving from the area near the east-side window to the west wall area (the west side of the main activity area in (Figure 9). (2) The enhancement of indoor surface reflectance significantly boosts the circadian stimulus, particularly in areas not directly illuminated by daylight: for type I dwellings, at a WWR of 0.3, the minimum CS notably increases from 0.04 to 0.12, and for type L dwellings, it rises from 0.05 to 0.17, solely by changing the reflectance; similarly, at a WWR of 0.7, for type I dwellings, the minimum CS escalates from 0.06 to 0.23, and for type L dwellings, from 0.11 to 0.28, effectively diminishing the "circadian darkness" areas. (3) A rise in WWR notably enhances the circadian stimulus, particularly near the window where the CS value sees a substantial rise. However, for the west side area, lacking direct daylight, the increase in CS for type I dwellings is from 0.06 to 0.12 with changes in WWR and albedo, the latter representing a 200% increase from the former; for type L dwellings, the increments are 0.06 and 0.11 respectively, with the latter being 183% of the former increase. In this simulation scope, the impact of changing WWR is less significant compared to altering reflectance, and an excessive WWR might also lead to increased glare risks.

Table 6. Under the three window-to-wall ratios; Combinations of ρ wall, ρ ceiling, and ρ floor values used in simulation.

Parameters	Avg. ρ Wall	Avg. ρ Floor	Avg. ρ Ceiling	"I" Shaped Plane			"L" Shaped Plane		
				WWR = 0.3 $\rho/(1-\rho')$	WWR = 0.5 $\rho/(1-\rho')$	WWR = 0.7 $\rho/(1-\rho')$	WWR = 0.3 $\rho/(1-\rho')$	WWR = 0.5 $\rho/(1-\rho')$	WWR = 0.7 $\rho/(1-\rho')$
Preset parameters	0.40	0.20	0.40	0.30	0.30	0.30	0.31	0.31	0.31
	0.40	0.20	0.60	0.33	0.33	0.33	0.33	0.33	0.33
	0.40	0.20	0.80	0.37	0.37	0.37	0.36	0.37	0.37
	0.40	0.40	0.40	0.67	0.67	0.67	0.67	0.67	0.67
	0.40	0.40	0.60	0.74	0.74	0.74	0.73	0.73	0.73
	0.40	0.40	0.80	0.82	0.83	0.84	0.80	0.81	0.82
	0.60	0.20	0.40	0.35	0.35	0.34	0.36	0.36	0.35
	0.60	0.20	0.60	0.39	0.39	0.38	0.40	0.40	0.39
	0.60	0.20	0.80	0.44	0.44	0.43	0.44	0.44	0.44
	0.60	0.40	0.40	0.78	0.77	0.77	0.80	0.79	0.78
	0.60	0.40	0.60	0.88	0.87	0.87	0.89	0.88	0.88
	0.60	0.40	0.80	1.00	1.00	1.00	1.00	1.00	1.00
	0.80	0.20	0.40	0.41	0.40	0.40	0.44	0.43	0.42
	0.80	0.20	0.60	0.47	0.46	0.45	0.50	0.49	0.48
	0.80	0.20	0.80	0.54	0.53	0.52	0.57	0.56	0.55
	0.80	0.40	0.40	0.93	0.92	0.90	0.99	0.97	0.95
	0.80	0.40	0.60	1.08	1.06	1.05	1.14	1.12	1.10
	0.80	0.40	0.80	1.27	1.26	1.25	1.33	1.31	1.29
Simulation model									

(a) "I" shaped simulation model   (b) "L" shaped simulation model

The primary factors contributing to the significant variation in circadian stimulus (CS) effects due to differing window-to-wall ratio (WWR) and albedo are as follows: High CS near windows is primarily due to direct light, which is influenced mainly by the intensity of direct light and WWR, and to a lesser extent, by indoor surface albedo. In contrast, CS deeper inside the room (e.g., on the west side of the main activity area) is largely the result of indirect light, highly reliant on indoor surface albedo. For instance, in L-type residential dwellings, maximum indoor reflectance can provide an adequate circadian stimulus in most activity areas (Figure 9b), even with a smaller WWR of 0.3.
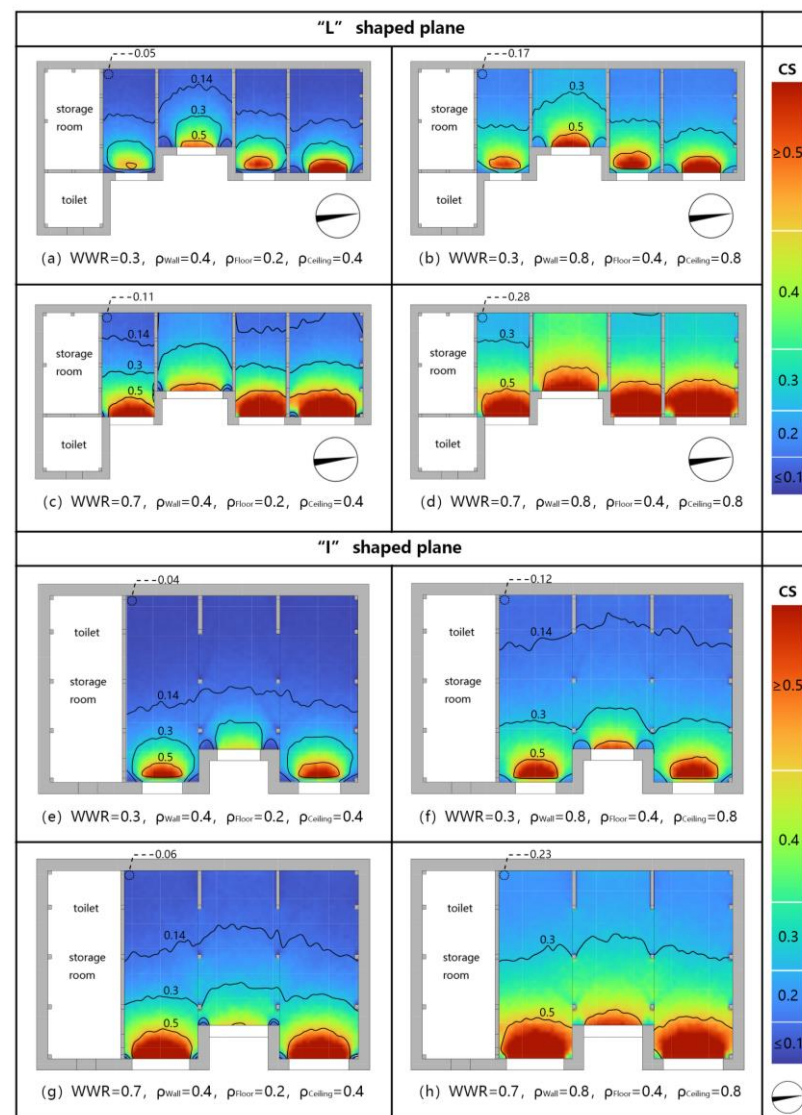
Figure 9. Distribution of CS in the main activity areas within a residential home under two typical models, I and L, two reflectance and two window-to-wall ratio settings.

4.2.2. Validation of Simplified Fitting Models

To further examine the variation in CS values across entire dwellings with different WWR and albedo, and to validate the proposed fitted mathematical model's accuracy (Equation (5)), we analyzed the overall CS of the two dwelling types using WWR and the ratio $\rho/(1 - \rho')$. The fitting results are depicted in (Figure 10).

(1) The streamlined model exhibits a strong correlation with the experimental data, achieving an R2 (Goodness of Fit) ranging from 0.964 to 0.983 at a WWR of 0.3; for a WWR of 0.5, the R2 is between 0.954 and 0.976; and for a WWR of 0.7, it lies between 0.939 and 0.972.

(2) Across six fittings, with a ρ of 0.2, the derived K·WWR (Equation (5)) values are 0.31, 0.33, 0.34, 0.32, with a minimal deviation of −4% and a maximal deviation of 5.3% from the mean. When ρ is set at 0.4, the resulting K·WWR values are 0.144, 0.145, 0.14, 0.141, showing a minimum deviation of −1.9% and a maximum of 2.9% from the average.
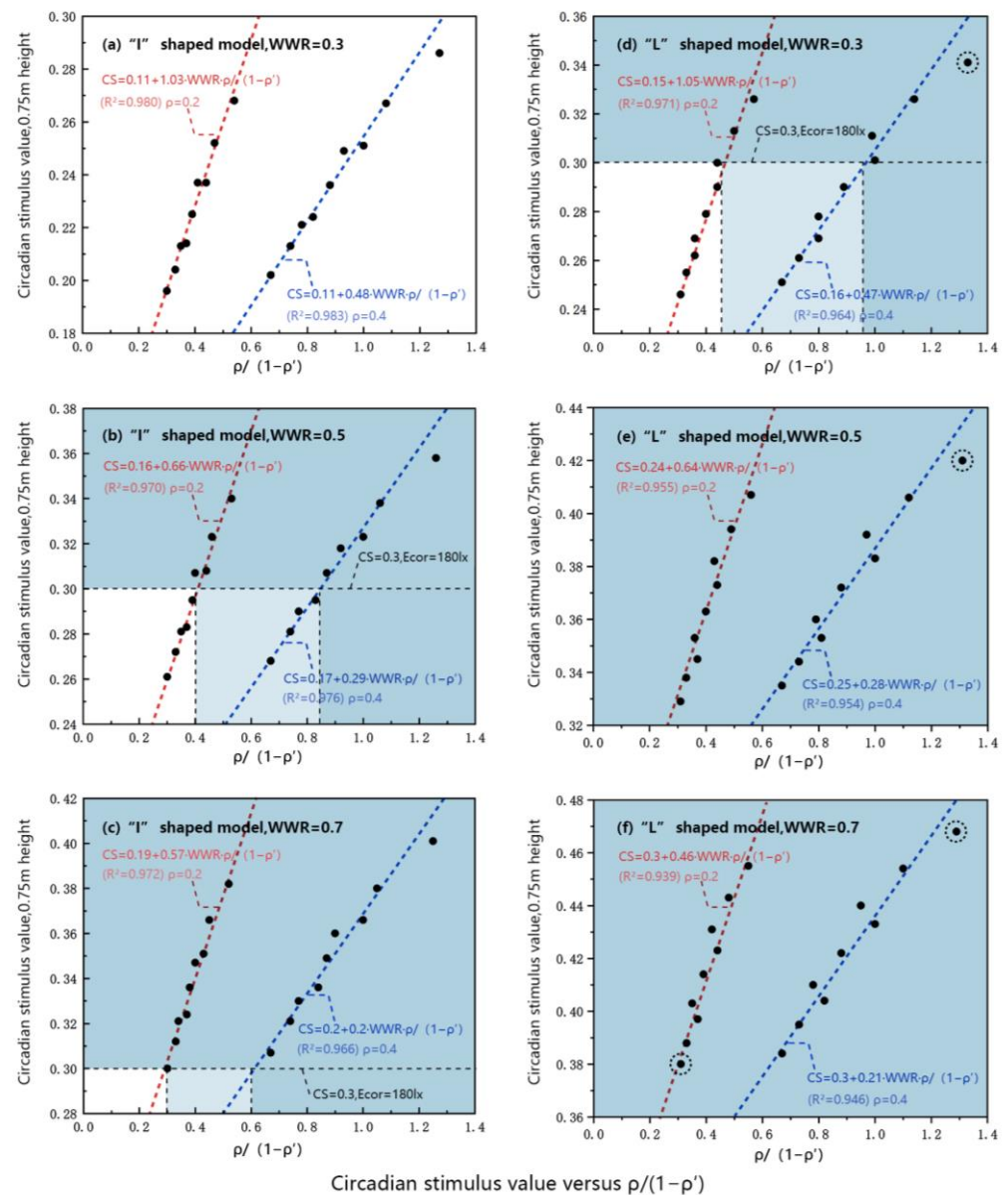
Figure 10. Relationship between circadian stimulus values and $\rho/(1 - \rho')$ for different window-to-wall ratios.

The accuracy of the fitted model is validated by result (1), confirming its precision. Moreover, result (2) demonstrates a negative correlation between K-WWR and the reflectance (ρ) of the primary reflective surface. Furthermore, (Figure 10) reveals that the indirect component of the circadian stimulus (CS (i)) linearly depends on the combination of WWR and $\rho/(1 - \rho')$. (Equation (5)) further illustrates that CS (i) has a super-linear relationship with ρ', suggesting a sublinear correlation between CS (i), WWR, and ρ'. This indicates the predominant influence of ρ' in achieving a high CS.

Within the defined simulation parameters, the top three CS (i) values are consistently achieved at the highest level of indoor weighted surface reflectance. Specifically, with a ρ' of 0.69, the $K \cdot WWR \cdot \rho/(1 - \rho')$ values are 0.19, 0.18, and 0.19, corresponding to WWRs of 30%, 50%, and 70%. In contrast, at a lower ρ' of 0.35 and a WWR of 70%, the $K \cdot WWR \cdot \rho/(1 - \rho')$ value drops to 0.09, as illustrated in (Figure 10d–f).

In optimizing traditional residential circadian daylighting design, particularly for rooms with substantial depth, adjusting the WWR and applying high-albedo white paint

is an effective approach to enhance circadian stimulation. The retrofitting strategies, as outlined in (Figure 10), include:

(1) For L-type residences with a WWR of 0.3, if the first reflective surface has a reflectance of 0.2, the indoor surface's weighted reflectance should exceed 0.57. With a reflectance of 0.4, it should be above 0.59. I-type residences may not meet these criteria.

(2) With a WWR of 0.5, I-type residences require an indoor surface weighted reflectance above 0.52 when the first reflective surface has a 0.2 reflectivity, and above 0.53 when it is 0.4. L-type residences generally meet these requirements.

(3) For a WWR of 0.7, I-type residences need an indoor surface weighted albedo over 0.33 with a first reflective surface albedo of 0.2, and over 0.35 with an albedo of 0.4. L-type residences satisfy these conditions.

5. Conclusions

As the aging population continues to grow, there is an increasing focus on health-related circadian issues among the elderly. The mobility of elderly individuals often results in insufficient daily corneal illumination to support a healthy circadian. This research aims to establish the correlation between circadian and daylight design parameters, offering practical guidance for interior circadian design in traditional dwellings in western Hunan. Additionally, it seeks to promote the digitalization and informatization of traditional dwellings in western Hunan for preservation purposes, aiming to integrate these efforts with sustainable tourism and community development, which supports the local economy while preserving cultural heritage. The primary contributions can be summarized as follows:

1. Assessment of the current indoor lighting conditions and circadian impact in traditional Miao dwellings in western Hunan. Seasonal variations had limited effects on the duration of the optimal circadian stimulus throughout the year. However, in winter, the CS significantly dropped, with an average CS < 0.14 in all units and even lower values in main activity areas, indicating challenges for elderly individuals in obtaining a sufficient circadian stimulus during winter.

2. Implementation of a simplified fitting model to guide circadian design, with validation against simulation data from Climate Studio 1.9. This model primarily applies to the indirect circadian component and is suitable for daylighting scenarios. It provides a quick field tool for circadian design and promotes healthy circadian concepts.

3. Exploration of different combinations of daylight conditions using Climate Studio daylighting software, involving indoor surface-weighted reflectance, first-reflection surface reflectance, and WWR for two types of traditional dwellings in simulations. The study provides dwellings parameter ranges required to achieve an appropriate circadian stimulus in traditional Miao dwellings in western Hunan.

4. Highlighting the significance of indoor surface-weighted reflectance over WWR in improving the circadian stimulus. The super linear dependency of indirect circadian stimulation on indoor weighted reflectance implies that higher indoor reflectance can contribute significantly to circadian well-being, surpassing the impact of direct light. Moreover, changes in indoor weighted albedo primarily enhance the indirect component of corneal illuminance, aiding in glare reduction and avoiding window modifications, which would otherwise alter the traditional residential landscape. This approach facilitates a more uniform distribution of indoor circadian lighting, aligning with the unique characteristics of traditional Miao dwellings in western Hunan, characterized by substantial depth.

This paper provides a detailed assessment of the circadian rhythm performance within traditional Miao ethnicity residences in Xiangxi from both dynamic and static perspectives. The evaluation aims to obtain circadian rhythm metrics under extreme conditions to meet the minimum requirements for circadian rhythms in architectural renovations. The performance evaluation of circadian rhythms after architectural modifications was conducted under overcast conditions, thus presenting certain limitations, such as the inability to

assess visual factors such as daylight and glare within the building under these conditions. Given that the primary focus of this research is on circadian rhythms, it serves as the basis for studying the non-visual effects on the elderly population of the Miao ethnicity in Xiangxi. Daylight and glare represent two separate research domains of visual effects, and a thorough investigation of these visual parameters will be gradually conducted in subsequent studies.

Author Contributions: J.L. designed and conducted the study, analyzed the data, prepared the figures, and wrote the manuscript. Z.Z. and Z.L. supervised the work. J.L., L.X. and J.W. revised the manuscript. All authors have read and agreed to the published version of the manuscript.

Institutional Review Board Statement: Not applicable to studies not involving humans or animals.

Informed Consent Statement: Informed consent was obtained from all subjects involved in the study.

Data Availability Statement: All data were generated by the author's field collection and software simulation.

Conflicts of Interest: The authors declare no conflict of interest.

References

1. Publicity Department of the CPC Central Committee Held a Press Conference on Measures and Achievements for High-Quality Development of Housing and Urban and Rural Development in the New Era. 2022. Available online: https://www.mohurd.gov.cn/xinwen/jsyw/202209/20220915_768000.html (accessed on 15 September 2023).
2. Sun, J.; Peng, B.; Wang, C.C.; Chen, K.; Zhong, B.; Wu, J. Building displacement measurement and analysis based on UAV images. *Autom. Constr.* **2022**, *140*, 104367. [CrossRef]
3. Bouzas, Ó.; Cabaleiro, M.; Conde, B.; Cruz, Y.; Riveiro, B. Structural health control of historical steel structures using HBIM. *Autom. Constr.* **2022**, *140*, 104308. [CrossRef]
4. Fu, J.; Zhou, J.; Deng, Y. Heritage values of ancient vernacular residences in traditional villages in Western Hunan, China: Spatial patterns and influencing factors. *Build. Environ.* **2021**, *188*, 107473. [CrossRef]
5. Xu, J.; Lu, Z.; Huo, X. The evolution and adaptive development of traditional dwelling in Southern Shaanxi, China. *Environ. Sci. Pollut. Res.* **2019**, *26*, 13914–13930. [CrossRef]
6. Agnihotri, S. Greying China: Challenges and solutions. In *Modern China*; Routledge India: London, UK, 2019.
7. Zhang, X. The Application of Spatial Information Technology in the Rural Elderly Care Model under the Strategy of "Building a Country with a Strong Transportation Network" in China. *Transp. Res. Procedia* **2022**, *61*, 481–486. [CrossRef]
8. Zhang, M.; You, S.; Zhang, L.; Zhang, H.; Wang, Y. Dynamic Analysis of the Effects of Aging on China's Sustainable Economic Growth. *Sustainability* **2023**, *15*, 5076. [CrossRef]
9. Barron, G.C.; Laryea-Adjei, G.; Vike-Freiberga, V.; Abubakar, I.; Dakkak, H.; Devakumar, D.; Johnsson, A.; Karabey, S.; Labonté, R.; Legido-Quigley, H.; et al. Safeguarding people living in vulnerable conditions in the COVID-19 era through universal health coverage and social protection. *Lancet Public Health* **2022**, *7*, e86–e92. [CrossRef]
10. Kuppusamy, P.P.; Bhatia, A.; Verma, A.; Shah, N.R.; Pratyush, P.; Shanmugarajan, V.; Kim, S.C.; Poongavanam, G.; Duraisamy, S. Accumulation of biomedical waste during the COVID-19 pandemic: Concerns and strategies for effective treatment. *Environ. Sci. Pollut. Res.* **2022**, *29*, 55528–55540. [CrossRef]
11. Alvis, B.D.; Hughes, C.G. Physiology Considerations in Geriatric Patients. *Anesth. Clin.* **2015**, *33*, 447–456. [CrossRef] [PubMed]
12. Emens, J.S.; Burgess, H.J. Effect of Light and Melatonin and Other Melatonin Receptor Agonists on Human Circadian Physiology. *Sleep Med. Clin.* **2015**, *10*, 435–453. [CrossRef] [PubMed]
13. Blume, C.; Garbazza, C.; Spitschan, M. Effects of light on human circadian rhythms, sleep and mood. *Somnologie* **2019**, *23*, 147–156. [CrossRef]
14. Boyce, P.R. *Human Factors in Lighting*; CRC Press: Boca Raton, FL, USA, 2014. [CrossRef]
15. Jamrozik, A.; Clements, N.; Hasan, S.S.; Zhao, J.; Zhang, R.; Campanella, C.; Loftness, V.; Porter, P.; Ly, S.; Wang, S.; et al. Access to daylight and view in an office improves cognitive performance and satisfaction and reduces eyestrain: A controlled crossover study. *Build. Environ.* **2019**, *165*, 106379. [CrossRef]
16. Westland, S.; Pan, Q.; Lee, S. A review of the effects of colour and light on non-image function in humans. *Color. Technol.* **2017**, *133*, 349–361. [CrossRef]

17. St Hilaire, M.A.; Gooley, J.J.; Khalsa, S.B.S.; Kronauer, R.E.; Czeisler, C.A.; Lockley, S.W. Human phase response curve to a 1 h pulse of bright white light. *J. Physiol.* **2012**, *590*, 3035–3045. [CrossRef]

18. Andersen, M.; Mardaljevic, J.; Lockley, S. A framework for predicting the non-visual effects of daylight—Part I: Photobiology—based model. *Light. Res. Technol.* **2012**, *44*, 37–53. [CrossRef]

19. Dijk, D.-J.; Lockley, S.W. Invited Review: Integration of human sleep-wake regulation and circadian rhythmicity. *J. Appl. Physiol.* **2002**, *92*, 852–862. [CrossRef]

20. Liu, M.; Shen, S.; Luo, X. The Application Strategy of Natural Light In Buildings For The Aged. *Chin. Hosp. Archit. Equip.* **2018**, *19*, 76–79.

21. Burns, A.C.; Saxena, R.; Vetter, C.; Phillips, A.J.; Lane, J.M.; Cain, S.W. Time spent in outdoor light is associated with mood, sleep, and circadian rhythm-related outcomes: A cross-sectional and longitudinal study in over 400,000 UK Biobank participants. *J. Affect. Disord.* **2021**, *295*, 347–352. [CrossRef]

22. Kim, S.J.; Lim, Y.C.; Suh, I.B.; Lee, J.H. Disrupted sleep maintenance is associated with altered circadian phase and phase angle in community-dwelling adults. *Sleep Med.* **2020**, *73*, 250–256. [CrossRef]

23. Lee, J.; Ma, K.; Moulik, M.; Yechoor, V. Untimely oxidative stress in β-cells leads to diabetes—Role of circadian clock in β-cell function. *Free Radic. Biol. Med.* **2018**, *119*, 69–74. [CrossRef]

24. Hamza, N.; Nagari, K. Assessment of Daylight in Relation to the Agitation Levels of People with Dementia. 2016. Available online: https://www.researchgate.net/publication/311101121 (accessed on 20 July 2023).

25. Figueiro, M.; Brons, J.; Plitnick, B.; Donlan, B.; Leslie, R. Measuring circadian light and its impact on adolescents. *Light. Res. Technol.* **2011**, *43*, 201–215. [CrossRef]

26. Karami, Z.; Golmohammadi, R.; Heidaripahlavian, A.; Poorolajal, J.; Heidarimoghadam, R. Effect of Daylight on Melatonin and Subjective General Health Factors in Elderly People. *Iran. J. Public Health* **2016**, *45*, 636–643.

27. Onega, L.L.; Pierce, T.W.; Epperly, L. Effect of Bright Light Exposure on Depression and Agitation in Older Adults with Dementia. *Issues Ment. Health Nurs.* **2016**, *37*, 660–667. [CrossRef]

28. Walker, W.H.; Walton, J.C.; DeVries, A.C.; Nelson, R.J. Circadian rhythm disruption and mental health. *Transl. Psychiatry* **2020**, *10*, 28. [CrossRef]

29. Hung, S.-M.; Milea, D.; Rukmini, A.V.; Najjar, R.P.; Tan, J.H.; Viénot, F.; Dubail, M.; Tow, S.L.C.; Aung, T.; Gooley, J.J.; et al. Cerebral neural correlates of differential melanopic photic stimulation in humans. *Neuroimage* **2017**, *146*, 763–769. [CrossRef]

30. Souman, J.L.; Tinga, A.M.; te Pas, S.F.; van Ee, R.; Vlaskamp, B.N.S. Acute alerting effects of light: A systematic literature review. *Behav. Brain Res.* **2018**, *337*, 228–239. [CrossRef]

31. Babilon, S.; Beck, S.; Khanh, T. A field test of a simplified method of estimating circadian stimulus. *Light. Res. Technol.* **2022**, *54*, 459–473. [CrossRef]

32. Wang, S.; Zhao, J. New prospectives on light adaptation of visual system research with the emerging knowledge on non-image-forming effect. *Front. Built. Environ.* **2022**, *8*, 1019460. [CrossRef]

33. Busatto, N.; Mora, T.D.; Peron, F.; Romagnoni, P. Application of Different Circadian Lighting Metrics in a Health Residence. *J. Daylighting* **2020**, *7*, 13–24. [CrossRef]

34. Mariana, G.; Figueiro, M.S.R. A Working Threshold for Acute Nocturnal Melatonin Suppression from "White" Light Sources used in Architectural Applications. *J. Carcinog. Mutagen.* **2013**, *4*, 150–155.

35. Lucas, R.J.; Peirson, S.N.; Berson, D.M.; Brown, T.M.; Cooper, H.M.; Czeisler, C.A.; Figueiro, M.G.; Gamlin, P.D.; Lockley, S.W.; O'hagan, J.B.; et al. Measuring and using light in the melanopsin age. *Trends Neurosci.* **2014**, *37*, 1–9. [CrossRef]

36. Rea, M.; Figueiro, M.; Bierman, A.; Hamner, R. Modelling the spectral sensitivity of the human circadian system. *Light. Res. Technol.* **2012**, *44*, 386–396. [CrossRef]

37. Rea, M.; Figueiro, M. Light as a circadian stimulus for architectural lighting. *Light. Res. Technol.* **2018**, *50*, 497–510. [CrossRef]

38. Figueiro, M.; Nagare, R.; Price, L. Non-visual effects of light: How to use light to promote circadian entrainment and elicit alertness. *Light. Res. Technol.* **2018**, *50*, 38–62. [CrossRef]

39. Dai, Q.; Huang, Y.; Hao, L.; Lin, Y.; Chen, K. Spatial and spectral illumination design for energy-efficient circadian lighting. *Build. Environ.* **2018**, *146*, 216–225. [CrossRef]

40. Konis, K. Field evaluation of the circadian stimulus potential of daylit and non-daylit spaces in dementia care facilities. *Build. Environ.* **2018**, *135*, 112–123. [CrossRef]

41. Acosta, I.; Leslie, R.; Figueiro, M. Analysis of circadian stimulus allowed by daylighting in hospital rooms. *Light. Res. Technol.* **2017**, *49*, 49–61. [CrossRef]

42. Cai, W.; Yue, J.; Dai, Q.; Hao, L.; Lin, Y.; Shi, W.; Huang, Y.; Wei, M. The impact of room surface reflectance on corneal illuminance and rule-of-thumb equations for circadian lighting design. *Build. Environ.* **2018**, *141*, 288–297.

43. Potočnik, J.; Cadena, J.D.B.; Košir, M.; Poli, T. Occupant perception of spectral light content variations due to glazing type and internal finish. *IOP Conf. Ser. Earth Environ. Sci.* **2019**, *296*, 012033. [CrossRef]

44. Potočnik, J.; Košir, M. In Situ Determined Circadian and Visual Daylighting Potential of an Office. In Proceedings of the International Conference on Sustainable Built Environment, SBE19 Seoul, Seoul, Republic of Korea, 12–13 December 2019. [CrossRef]

45. Yao, Q.; Cai, W.; Li, M.; Hu, Z.; Xue, P.; Dai, Q. Efficient circadian daylighting: A proposed equation, experimental validation, and the consequent importance of room surface reflectance. *Energy Build.* **2020**, *210*, 109784. [CrossRef]

46. Stroner, M.; Kremen, T.; Braun, J.; Urban, R.; Blistan, P.; Kovanic, L. Comparison of 2.5D Volume Calculation Methods and Software Solutions Using Point Clouds Scanned before and after Mining. *Acta Montan. Slovaca* **2019**, *24*, 296–306.

47. Thacker, B.H.; Doebling, S.W.; Hemez, F.M.; Anderson, M.C.; Pepin, J.E.; Rodriguez, E.A. *Concepts of Model Verification and Validation*; Los Alamos National Lab.: Los Alamos, NM, USA, 2004. [CrossRef]

48. EnergyPlus, The U.S. Department of Energy. Available online: https://energyplus.net (accessed on 21 July 2023).

49. Sui, G.; Liu, J.; Leng, J.; Yu, F. Daylighting performance assessment of traditional skywell dwellings: A case study in Fujian, China. *J. Build. Eng.* **2023**, *68*, 106028. [CrossRef]

50. *GB/T 5699-2017*; Method of Daylighting Measurements. Standards Press of China: Beijing, China, 2017. (In Chinese)

51. *GB 10000-1988*; Human Dimensions of Chinese Adults. Standards Press of China: Beijing, China, 2021. (In Chinese)

52. Quek, G.; Jakubiec, J.A. Calibration and Validation of Climate-Based Daylighting Models Based on One-Time Field Measurements: Office Buildings in the Tropics. *Leukos* **2021**, *17*, 75–90. [CrossRef]

53. Jones, N.L.; Reinhart, C.F. Experimental validation of ray tracing as a means of image-based visual discomfort prediction. *Build. Environ.* **2017**, *113*, 131–150. [CrossRef]

54. Bellia, L.; Seraceni, M. A proposal for a simplified model to evaluate the circadian effects of light sources. *Light. Res. Technol.* **2014**, *46*, 493–505. [CrossRef]

55. Nagare, R.; Rea, M.S.; Plitnick, B.; Figueiro, M.G. Nocturnal Melatonin Suppression by Adolescents and Adults for Different Levels, Spectra, and Durations of Light Exposure. *J. Biol. Rhythm.* **2019**, *34*, 178–194. [CrossRef]

56. Acosta, I.; Navarro, J.; Sendra, J.J. Towards an Analysis of Daylighting Simulation Software. *Energies* **2011**, *4*, 1010–1024. [CrossRef]

57. Dai, Q.; Cai, W.; Shi, W.; Hao, L.; Wei, M. A proposed lighting-design space: Circadian effect versus visual illuminance. *Build. Environ.* **2017**, *122*, 287–293. [CrossRef]

58. Dai, Q.; Cai, W.; Hao, L.; Shi, W.; Wang, Z. Spectral optimisation and a novel lighting-design space based on circadian stimulus. *Light. Res. Technol.* **2018**, *50*, 1198–1211. [CrossRef]

59. *EN 12464-1-2011*; Lighting of Work Places. Standards Press of CEN: Brussels, Belgium, 2010.

60. *GB 50189-2005*; Design Standard for Energy Efficiency of Public Buildings. Standards Press of China: Beijing, China, 2005. (In Chinese)